FLASH LiDAR SINGLE PHOTON IMAGING OVER 50 KM

Z. Q. Xia [1] *

[1] Beijing Institute of Space Mechanics & Electricity, Beijing, China - xiazhongqiu@126.com

KEY WORDS: Flash LiDAR, Single photon imaging, Photon counting, Vertical cavity surface emitting laser, Single photon avalanche diode, Space-borne.

ABSTRACT:

In order to demonstrate the feasibility of single-photon imaging of flash lidar in the permanent shadow area of the moon, a set of space-based single-photon imaging system is designed, including the lidar based on VCSEL array, the optical emitting system based on the uniform beam shaping meta-lens using propagation phase and geometric phase joint control method, the two-axis three-mirror optical receiving system, and the single-photon detector array based on photon counting mode. According to the heavy-tailed pulse laser function, Poisson statistical filtering theory and Monte Carlo simulation method, the echo photon number, the photon counting process, the ranging accuracy and the intensity image are simulated in the condition of 50 km detection distance by setting different of the object reflectivity, the repetition times and the gating interval time. The results show that according to the parameter settings in this paper, the number of echo photons is as low as about 10^{-4} orders. However, the photon counting waveform can better restore the transmission waveform. The setting of the repetition number and the gating interval time should not only consider the missing detection phenomenon, but also consider the noise accumulation. When the repetition number is 2000 and the gate number is 200, the ranging accuracy can reach 0.075m, and the imaging in the crater without light is realized.

1. INTRODUCTION

1.1 Background and Importance

Since the launch of human lunar exploration activities, many important research results have been achieved, among which the extreme exploration of the permanent shadow area of the south pole of the moon has gradually become a hot spot in recent years. The permanent shadow area cannot be illuminated by the sun, and there is only some diffuse reflected light from the surrounding non-shadow area. The high-sensitivity terrain camera of the Selenological and Engineering Explore (SELENE) achieves the intensity imaging of the crater by increasing the exposure time under the specific timing conditions (Haruyama et al., 2008). And the lunar orbiter laser altimeter (LOLA) instrument of the Lunar Reconnaissance Orbiter (LRO) achieves the range imaging (Mazarico et al., 2011). The Lunar Flashlight (LF) will carry an active multi-band reflectometer based on an optical receiver aligned with four high power diode lasers to measure the reflectance of the lunar surface of water ice (Vinckie et al., 2019). The passive imaging scheme based on the sunlight is technically difficult and has many constraints. For deep crater with complex terrain in permanent shadow areas, the intensity and range information acquisition simultaneously will become particularly difficult.

1.2 Research Status

Single-photon imaging technology irradiates the target with high repetition rate pulse laser and records the emission time. When the number of echo photons is very small, it uses a large-aperture optical lens for collection, completes photoelectric conversion through a single-photon detector, generates an avalanche signal, records the arrival time of photons, and records the number of signals by a photon counter. In this way, the light intensity information and distance information of the target can be accumulated based on Poisson statistics by increasing the number of repetitions, so as to realize the grayscale imaging and three-dimensional imaging of the target. Compared with traditional imaging methods, the number of photons required has been reduced from about 10^4 to 10, and the system sensitivity has been greatly improved, which has a huge advantage in the application of remote dim target information acquisition (Xia et al., 2022).

Since the first photon imaging system was proposed by the Ahmed Kirmani team of MIT in 2014 (Kirmani et al., 2014), the Xu Feihu team of the University of Science and Technology of China achieves single-photon imaging at a distance of more than 200 km in 2021(Li et al., 2021). The single-photon imaging distance has broken through to the order of 100 km. The space-based application of single-photon imaging technology has become possible.

1.3 Research Contents

Unlike the interpolation fitting method based on the point target ranging data, the flash LiDAR has the characteristics of high-speed imaging and three-dimensional reconstruction of surface targets without the scan mechanism. However, there are also some disadvantages about this observation mode. Because of the far distance of the space-borne detection, the light intensity of the area light source will decrease rapidly. And the intensity of the light reaching the focal plane array must be uniform enough. In addition, the amount of the photon counting data based on the high repetition rate pulsed laser is huge. So, it is necessary to set the laser repetition frequency and the gating number reasonably. In this paper, we design a flash LiDAR system based the vertical cavity surface emitting laser (VCSEL) source, the meta-lens and the single photon avalanche diode (SPAD) array. The range imaging and intensity imaging scheme is studied and the image performance is simulated.

2. PRINCIPLE AND MODELS

2.1 System Overview

The detection system consists of the objective, the active lighting system (including the pulse laser, the collimation lens

* Corresponding author

and the meta-lens) and the optical receive system (including the Cassegrain optical system, the SPAD array and the photon counter) as shown in the Fig 1. During imaging, the target, the lighting system and the receiving system are relatively static. Because there is no scanning component, the imaging speed is faster than that of the mechanical rotating LiDAR and the micro electro mechanical system (MEMS) based LiDAR, and the structure is simpler than that of optical phase array (OPA) LiDAR. Therefore, laser radar is very suitable for space-based detection.

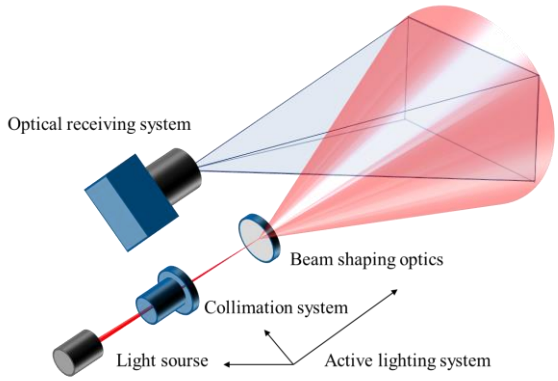

Figure 1. Flash LiDAR detection principle.

2.2 Objective Characteristic

Firstly, the illumination at the south pole of the moon is analysed. As shown in Fig 2, the angle between the sunlight direction and the lunar surface is approximately zero. For permanent shaded areas, there is no light in the lunar crater throughout the year, which means that the background noise caused by the photons of the reflect sunlight can be ignored.
To verify the flash LiDAR imaging performance, several objects with high reflectivity (0.4, 0.7, 0.8 and 0.9) are placed in the crater model, and other places is set to less than 0.1.

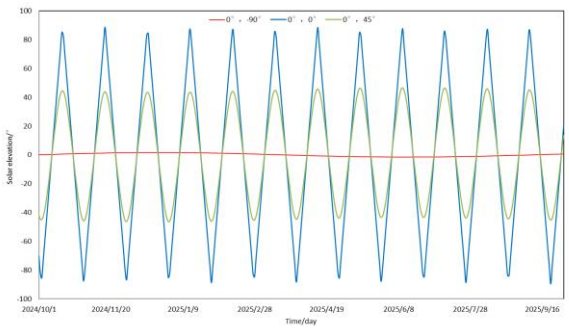

Figure 2. Changes of the sun elevation angle at different positions on the lunar surface within one year.

2.3 Active Lighting System

The active lighting system consists of the pulse VCSEL array, the collimation lens and the meta-lens as shown in Fig 3. The detection range of the flash LiDAR can be increased by improving the out power of the active lighting system. There are three specific ways: (1) Increase the VCSEL luminous dots, but this cannot be unlimited. When the dots reach a certain level, it requires a large input current introducing a large heat in the VCSEL chip which cannot be dissipated. (2) Magnify the luminous aperture of a single unit, but this method also has a certain upper limit due to the restriction of the current carrying distribution loss and the modal characteristics. (3) Adjust the VCSEL unit of single PN junction to the VCSEL unit of multiple PN junctions.

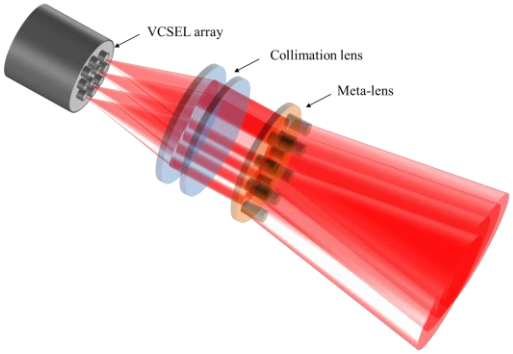

Figure 3. Active lighting system.

Considering the above, we choose the third method (adopting 5 PN junction VCSEL scheme) (Rowland et al., 2021). The VCSEL parameters are set as Table 1.

Table 1. VCSEL parameters.

Parameter	Nominal value
Wavelength /nm	1550
Power density /W/mm^2	1400
Luminous area /μm^2	250×250
Temperature drift nm/℃	0.07

The emission power of active lighting system is the product of the power density and the luminous area.

$$P=PD\cdot S \quad (1)$$

$$S=\pi[D\cdot tan(\theta/2)]^2 \quad (2)$$

where P = out power
PD= power density
S = luminous area
D=distance
θ =laser divergence angle

In order to maximize the use of the laser energy, a 25.6m×25.6m rectangular light spot with uniform illumination can be obtained at the detection distance of 50km by setting the collimation lens and the meta-lens parameters as Table 2. The propagation phase and Pancharatnam-Berry (PB) phase control methods are used in the meta-lens design. Finally, it is designed to be suitable for 1550nm wavelength and control the propagation direction by scanning the radius and the height of the cylinder (Khorasaninejad et al., 2016).

Table 2. Collimation lens and the meta-lens parameters.

Parameter	Nominal value
Wavelength /nm	1550
Focal length /m	0.49
F#	0.4
Divergence angle/°	0.04

2.4 Optical Receiving System

A two axis three mirrors (the primary mirror, the secondary mirror and the tertiary mirror) optical system based on Cassegrain system is adopted as shown in Fig 4. A 45° plane mirror is set in the diagonal direction of the main mirror and the three mirror, of which the centre has an opening that makes the

optical system form a circular field of view. The exit pupil is designed near the centre hole to minimize the size of the opening (Wang et al., 2022).

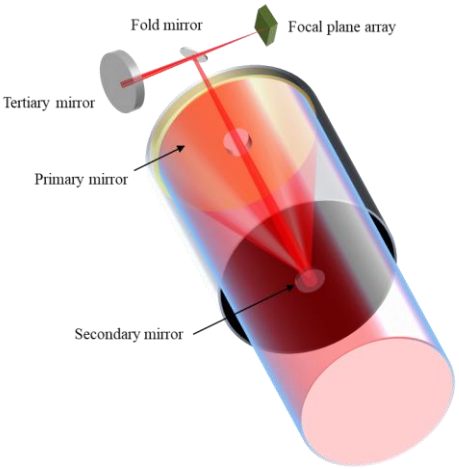

Figure 4. Optical receiving system.

Considering the modulation transfer function of the optical system at Nyquist frequency. The optical system parameters are set as Table 3.

Table 3. Optical system parameters.

Parameter	Nominal value
Focal length /m	5
F#	9
Field of view/°	0.03
Transmittance	0.9

The light reflected from the tertiary mirror passes through the central hole of the plane mirror and hits the focal plane. Because of the high detection efficiency at 1550nm wavelength (Comandar et al., 2015), the InGaAs/InP Single photon avalanche diode (SPAD) array is adopted to receive the tiny amounts of photons reflected from the objective, of which the parameters are set as Table 4. Based on Poisson statistical filtering theory, the strength and time information of the signal is recorded by controlling the gating interval and increasing the number of the repetitions.

Table 4. SPAD parameters.

Parameter	Nominal value
Wavelength/nm	900-1700
Array size	128×128
Pixel size /μm	20
Filling factor	0.6
Photon detection efficiency	30%
Dark count rate /kHz	2000
Dead time /ns	100
Time jitter /ps	50

3. RESULTS AND ANALYSIS

3.1 Echo Photon Number

The echo photon number of the pulse laser in different albedo of the object are analysed by Monte Carlo simulation methods, as shown in Fig 5. By comparing the results of echo photon number in the same integration time such as Fig 5(a) to 5(d), it can be seen that the echo photon number is proportional to the reflectivity of the object, which is consistent with the reality. For the four reflectivity objects of 0.9, 0.8, 0.7 and 0.4, the number of echo photons is all very small, reaching the order of 10^{-4}, which is due to the weak illumination of the area source laser emitted by the flash lidar based on VCSEL array when reaching the object. In addition, the reduction degree of the echo waveform gradually decreases with the increase of gating interval as shown in Fig 5(a), Fig 5(e) and Fig 5(f). Limited by the current power level of VCSEL array laser, we decided to increase the pulse repetition rate and set the gating interval reasonably in the next work to improve the pulse echo photon count to achieve single-photon imaging at a distance of 50 km.

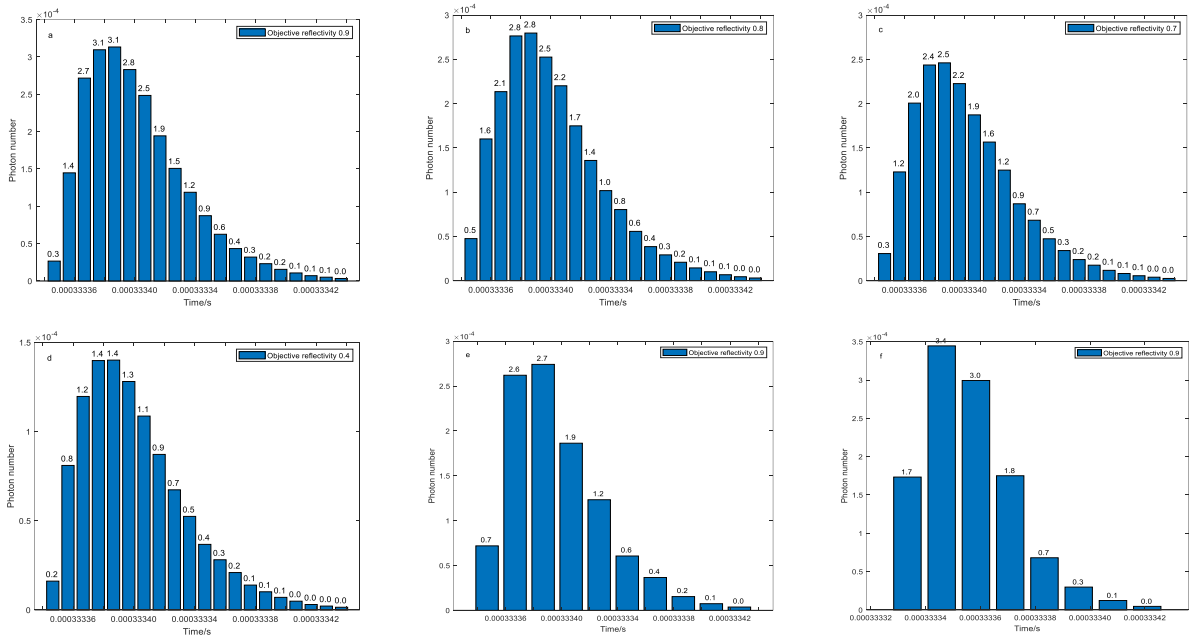

Figure 5. Echo photon number of different objective reflectivity. **a**. Objective reflectivity is 0.9, and gating interval is 0.05 μs. **b**. Objective reflectivity is 0.8, and gating interval is 0.05 μs. **c**. Objective reflectivity is 0.7, and gating interval is 0.05 μs. **d**. Objective

reflectivity is 0.4, and gating interval is 0.05 μs. **e**. Objective reflectivity is 0.9, and gating interval is 0.1 μs. **f**. Objective reflectivity is 0.9, and gating interval is 0.125 μs.

3.2 Gate number

Taking 50km orbital altitude as an example, the photon counting results of space pulse laser echo are simulated under different parameter settings using the Monte Carlo simulation method, as shown in Fig 6. The echo waveform is converted from analog state (continuous) to digital state (discontinuous), and the photon count value has a step in different door opening times. This is based on the results of Poisson statistics. As shown in Fig 6(a), the peak value of photon counting reaches about 90, but the waveform distortion occurs when the number of the gate number is set to 4. As the number of gates increases to 20 in Fig 6(b), the peak value of photon counting drops to about 30, and the degree of waveform reduction gradually increases, but the photon noise and dark count noise are still large. The gate number is increased to 200 in Fig(c), the peak value further decreased to about 12, and the photon counting caused by photon noise and dark count noise is reduced significantly. When the gate number continuous to increase to 2000 greater than the number of repetitions, the phenomenon of missing inspection occurs. The photon count does not occur in part of the door opening time.

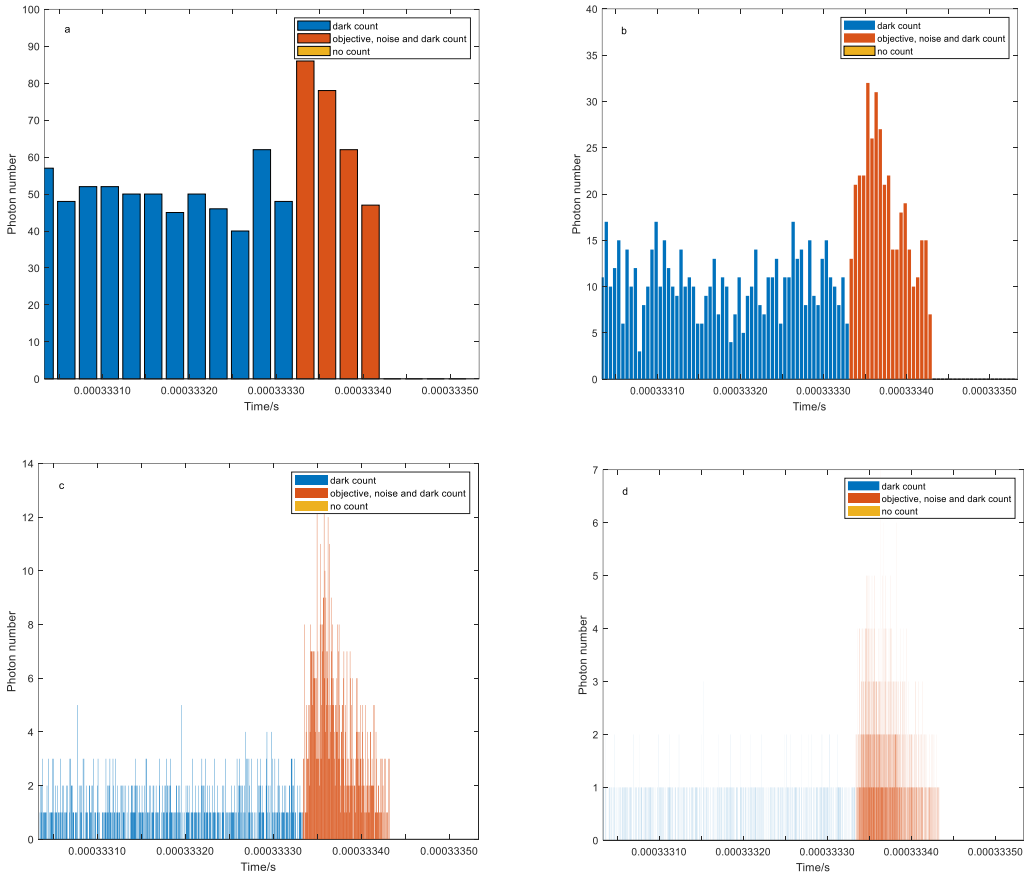

Figure 6. Photon counting results when the repetition is 1000. **a**. Gate number is 4. **b**. Gate number is 20. **c**. Gate number is 200. **d**. Gate number is 2000.

3.3 Photon Counting Process

Therefore, the repetition number is must set greater than the gate number. The photon counting results are shown in Fig 7, which also indicates the counting process with the counting number increasing. When the low repetition rate of 500 is adopted, the photon count caused by signal is slightly higher than that caused by noise, so it is difficult to distinguish between signal and noise as shown in Fig 7(a). When the number of repetitions increases to 1000 of Fig 7(b) and 1500 of Fig 7(c), the signal waveform gradually becomes obvious and is easy to distinguish. When the number of repetitions is set to 2000 and the number of gating is set to 200, the echo waveform is smoother and the photon count peak step is slower as shown in Fig 7(d). The dynamic range of single-photon imaging can be adjusted by adjusting the number of repetitions, but it also puts forward higher requirements for the development of pulse lasers and photon counters.

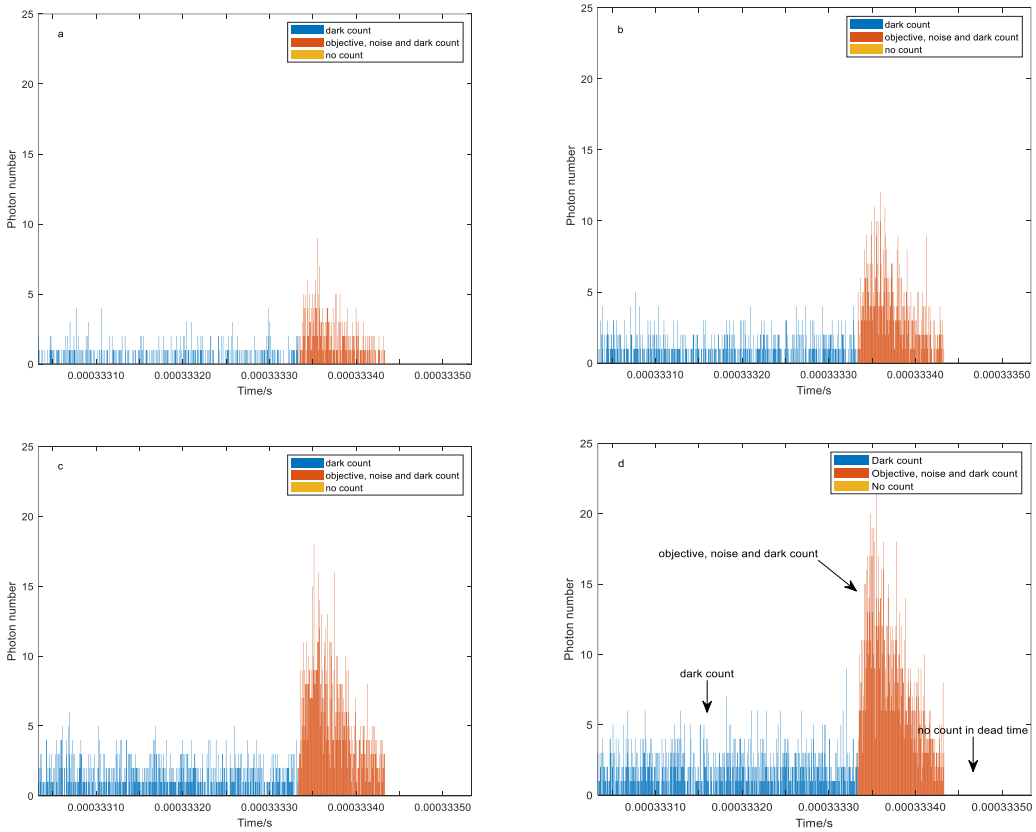

Figure 7. Photon counting process when the gate number is 200. **a**. Repetitions is 500. **b**. Repetitions is 1000. **c**. Repetitions is 1500. **d**. Repetitions is 2000.

3.4 Ranging accuracy

According to the above waveform simulation, it is difficult to determine the rising time of the echo waveform, so the photon counting peak time is used as the basis for determining the pulse echo time. The echo photon number of the pulse laser when gate number is set to 200 are simulated by Monte Carlo simulation methods, as shown in Fig 8. The corresponding gate position number at the peak value is 40.

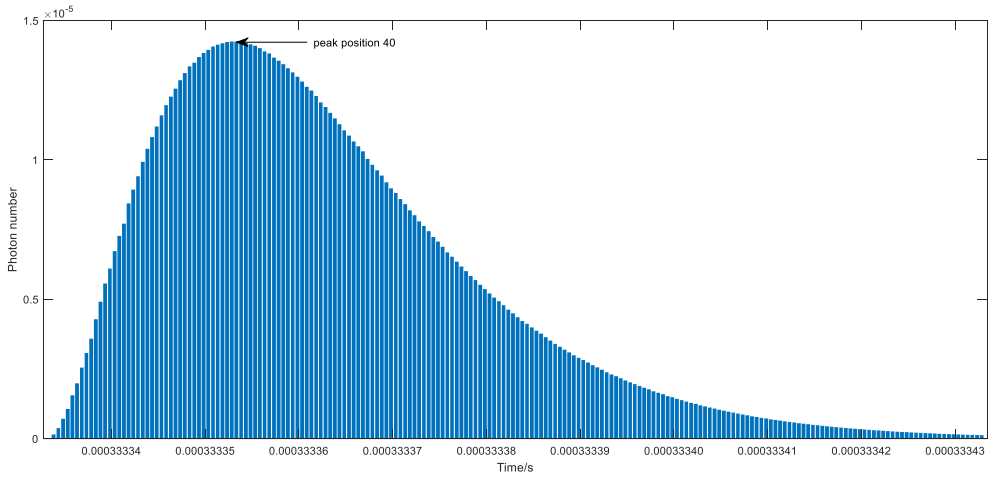

Figure 8. Photon number when the gate number is 200.

The simulation results of the peak size, position and ranging accuracy under the above four conditions are listed in Table 5. It can be seen that when the repetition rate increases from 500 to 2000, the ranging accuracy increases from 0.36m to 0.075m. Therefore, the ranging accuracy can be improved by increasing the laser repetition rate.

Table 5. Ranging accuracy simulation results.

Repetition	Gate number	Peak value	Peak position	Ranging accuracy/m
2000	200	22	45	0.075
1500	200	17	51	0.165
1000	200	12	53	0.195
500	200	9	64	0.360

3.5 Intensity image performance

According to the idea of first photon imaging method to retrieve the target reflectivity, the relative reflectivity of the target can be equivalent to the ratio of the number of recovered photons to the number of emitted photons (Kirmani et al., 2014). Therefore, the model of the permanent shadow crater at the South Pole is set to include three objects with reflectivity of 0.9, 0.7 and 0.4 to represent the ice water mixture, and the reflectivity of other places is set to 0.1 as shown in Fig 9(a). The simulation results of passive imaging using solar illumination are shown in the Fig 9(b). No object in the crater can be seen, only the approximate outline of the crater edge can be seen. Then the flash LiDAR single photon imaging method is used, and the result is shown in Fig9(c), which can be seen that the objects in the crater can be imaged. The echo photon counting number is different to the three kind of reflectivity objects, and for objects with the same reflectivity, the number of echo photons is also slightly different. For example, for objects with 0.9 reflectivity, the number of echo photons is 1459, 1564 and 1619 respectively. This is because photon counting method is a random probability statistical method.

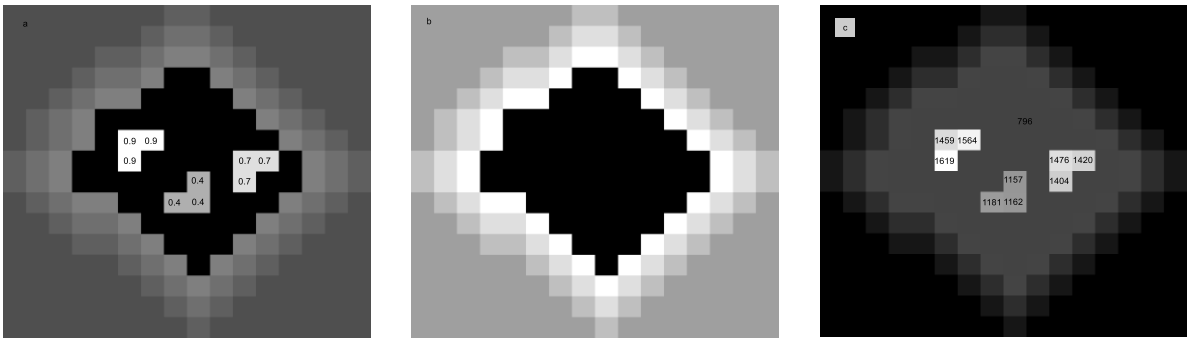

Figure 9. Intensity image. **a**. Real crater model including three objectives (the reflectivity is 0.9, 0.7 and 0.4 respectively). **b**. General image by sunlight. **c**. Flash LiDAR single photon image.

4. CONCLUSIONS

In order to solve the problem of long imaging range and weak signal in the permanent shadow area of the moon, obtain the continuous intensity image in the crater, and complete the crater depth measurement, a set of single-photon imaging lidar system is designed. The number of echo photons under different reflectivity conditions is simulated by Monte Carlo method. The photon counting process is simulated by setting different repetition frequencies and gating intervals. According to the photon counting results, taking into account the reduction degree of pulse laser echo waveform and noise accumulation in a compromise, we can adjust the repetition times, the gate interval time and other methods to improve the fidelity of echo waveform and the accuracy of echo time determination while avoiding the "missing detection" phenomenon.

In the detection of water ice mixture on the lunar surface, the reflectivity information is not enough to explain the existence of water ice mixture. In order to further identify the material types, the follow-up work can continue to increase the imaging spectrum of the flash lidar system, obtain sufficient spectral information of the ground objects, and improve the accuracy of the inversion of the lunar surface material.

REFERENCES

Haruyama, J., et al., 2008: Lack of Exposed Ice Inside Lunar South Pole Shackleton Crater. *Science*, 322, 938-939.

Mazarico, E., Neumann, G. A., Smith, D. E., et al., 2011: Illumination conditions of the lunar polar regions using LOLA topography. *Icarus*, 211(2), 1066-1081.

Vinckier, Q., et al., 2019: Design and Characterization of the Multi-Band SWIR Receiver for the Lunar Flashlight CubeSat Mission. Remote Sensing, 11, 440.

Xia, Z. Q., et al., 2022: Simulation Techniques of a Space-Borne Single-Photon Counting Imaging System. *Laser & Optoelectronics Progress*, 59(16), 1611001.

Kirmani, A., Venkatraman, D., Shin, D., et al., 2014: First-photon imaging. *Science*, 343(6166), 58-61.

Li, Z. P., Ye, J. T., Huang, X., et al., 2021: Single-photon imaging over 200 km. *Optica*, 8(3), 344-349.

Rowland, J., et al., 2021: Using an injection-locked VCSEL to produce Fourier-transform-limited optical pulses. *Optics Letters*, 46(2),412-415.

Khorasaninejad, M., et al., 2016: Metalenses at visible wavelengths Diffraction-limited focusing and subwavelength resolution imaging. *Science*, 352(6290), 1190-1194.

Wang, Y., et al., 2022: Optical design method of a three-mirror anastigmatic telescope with low misalignment sensitivity based on the nodal aberration theory. *Applied Optics*, 61(22), 6483-6491.

Comandar, L. C., et al., 2015: Gigahertz-gated InGaAs/InP single-photon detector with detection efficiency exceeding 55% at 1550 nm. Journal of Applied Physics, 117(8), 083109.

Kirmani, A., Venkatraman, D., Shin, D., et al., 2014: First-photon imaging. *Science*, 343(6166), 58-61.